

**${}^3\text{He}(n, \gamma){}^4\text{He}$  cross section and the photodisintegration of  ${}^4\text{He}$** 

R. J. Komar, H.-B. Mak, J. R. Leslie, and H. C. Evans  
*Physics Department, Queen's University, Kingston, Ontario,  
 Canada K7L 3N6*

E. Bonvin and E. D. Earle  
*Chalk River Laboratories, Chalk River, Ontario,  
 Canada K0J 1J0*

T. K. Alexander  
*PO Box 1634, Deep River, Ontario, Canada K0J 1P0*  
 (Received 2 July 1993)

The absolute cross section of the  ${}^3\text{He}(n, \gamma){}^4\text{He}$  reaction was measured at five energies between  $E_n=0.14\text{--}2.0$  MeV to an accuracy of  $\sim\pm 10\%$ . The  $\sim 21$  MeV gamma rays produced in a  ${}^3\text{He}$  gas target were detected at  $90^\circ$  with respect to the beam direction. The results are discussed in light of previous measurements of the two-body photodisintegration of  ${}^4\text{He}$ .

PACS number(s): 25.40.Lw, 27.10.+h, 25.20.Lj

**I. INTRODUCTION**

Charge symmetry has long been considered to be an important property of the nuclear force, and it is only recently that strong evidence of charge symmetry breaking (CSB) at the level of  $\sim 1\%$  has been found [1]. Historically, the study of mirror reactions has played an important role in the search for CSB in the nucleus. In 1957, Barker and Mann [2] suggested that the cross sections for proton and neutron emission from the excited state of a self-conjugate nucleus would be sensitive to the amount of isospin mixing in the state, and thus, to the presence of CSB components in the nuclear force. In particular, it was expected that the effects of CSB would be exhibited most clearly in photonucleon emission from an isospin  $T = 1$  state excited by an  $E1$  transition. In this respect, the photodisintegration of  ${}^4\text{He}$  over the region of the giant dipole resonance ( $E_\gamma=21\text{--}40$  MeV) has been studied in detail, as the  ${}^4\text{He}$  nucleus is relatively simple, and Coulomb interaction effects are small.

Conventional theoretical models for the  ${}^4\text{He}$  system [3–7] without CSB predict the ratio of the photonucleon cross sections  $R_\gamma=\sigma_{\gamma,p}/\sigma_{\gamma,n}$  to be  $\sim 1.1$  at  $E_\gamma=25\text{--}40$  MeV. Many measurements of  $\sigma_{\gamma,n}$  and  $\sigma_{\gamma,p}$  have been performed to test the theory (see [8] and the references therein for a recent list of the experiments). However, the experimental results vary widely, and the situation remains unclear. In particular, the  $(\gamma, n)$  peak cross section varies by as much as a factor of 2 between different experiments. A critical review of the experimental data obtained before 1983 was done by Calarco *et al.* [9]. Based heavily on the monoenergetic photon beam experiment of Berman *et al.* [10] and on the  ${}^3\text{He}(n, \gamma)$  capture data of Ward *et al.* [11], values for  $\sigma_{\gamma,n}$  were recommended that peak at  $\sim 1.1$  mb. The recommended values for  $\sigma_{\gamma,p}$  were based predominately on the  ${}^3\text{H}(p, \gamma)$  capture data of Perry and Bame [12], McBroom *et al.* [13], and Calarco

*et al.* [14], and peak at  $\sim 1.8$  mb [see [14] for a discussion of the  $(p, \gamma)$  data]. From these cross sections,  $R_\gamma$  was found to vary between 1.7 and 1.2 over the energy region  $E_\gamma=25\text{--}35$  MeV, in disagreement with the conventional theoretical predictions. It was suggested that a charge symmetry breaking component of the nuclear force was responsible for the large value of the ratio [9]. However, all direct measurements of the ratio  $R_\gamma$  [15–19] in which both photonucleon reactions were detected produced results consistent with unity, in disagreement with the conclusions of Calarco *et al.* [9].

Recently, Bernabei *et al.* [20] measured the  ${}^4\text{He}(\gamma, p)$  cross section at  $E_\gamma=28.6\text{--}58.1$  MeV in an experiment similar to that of Berman *et al.* [10]; that is, they used a monoenergetic photon beam, a gas target, and a  $\sim 4\pi$  particle detector. The results are lower than the values for  $\sigma_{\gamma,p}$  recommended by Calarco *et al.* [9], and if compared with the recommended values for  $\sigma_{\gamma,n}$  [9], produce a mean value of  $\langle R_\gamma \rangle = 1.01 \pm 0.06$  for energies of  $E_\gamma=28.6\text{--}42.4$  MeV. Feldman *et al.* [21] subsequently remeasured the  ${}^3\text{H}(p, \gamma)$  capture cross section at  $E_\gamma=21.3\text{--}31.1$  MeV, obtaining results  $\sim 35\%$  lower than the previous values [12–14] and confirming the results of Bernabei *et al.* [20]. Hence, these new results for  $\sigma_{\gamma,p}$ , if taken with the recommended values for  $\sigma_{\gamma,n}$  [9], produce a value of  $R_\gamma$  in agreement with the conventional theoretical predictions and the direct ratio measurements [15–19].

Although the  $(\gamma, n)$  [10,11] and  $(\gamma, p)$  [20,21] data now appear to be consistent, the situation is still far from clear. It is not known why the earlier  ${}^3\text{H}(p, \gamma)$  experiments [12–14] yielded higher results than the recent measurement by Feldman *et al.* [21]. In fact, the earlier results are corroborated by a new measurement of  $\sigma_{\gamma,p}$  and  $\sigma_{\gamma,n}$  by Nagornyy *et al.* [19], which yielded peak cross sections of 1.8 and 1.7 mb for the  $(\gamma, p)$  and  $(\gamma, n)$  reactions, respectively. Also, a recent measurement of the elastic photon scattering cross section on  ${}^4\text{He}$  by Wells *et al.* [22]

was used to deduce the sum  $(\sigma_{\gamma,p} + \sigma_{\gamma,n}) = 2.86 \pm 0.12$  mb at the peak in the giant dipole resonance, in excellent agreement with the peak value of  $2.90 \pm 0.16$  mb recommended by Calarco *et al.* [9]. However, the combination of the results for  $\sigma_{\gamma,p}$  [20,21] and the recommended values for  $\sigma_{\gamma,n}$  [9] that produce a ratio  $R_\gamma$  consistent with unity sum to a peak value of  $2.37 \pm 0.13$  mb, which is substantially lower than the result of Wells *et al.* [22]. The sum of the peak cross sections measured by Nagornyy *et al.* [19] is  $\sim 3.5$  mb, even higher than the elastic scattering result. Thus, there are contradictions among the latest measurements on the  $^4\text{He}$  system.

The present work describes a measurement of  $\sigma_{n,\gamma}$  at five energies of  $E_n = 0.14$ – $2.0$  MeV (corresponding to photon energies of  $E_\gamma = 20.7$ – $22.0$  MeV). Using the results of refined resonating group model calculations [7], the present results are extended to higher energies to allow comparison with the published results for  $\sigma_{\gamma,n}$  and the values recommended by Calarco *et al.* [9]. Additional details of the experiment are given in Refs. [23,24].

## II. APPARATUS

The targets and medium-energy gamma ray spectrometer used in the experiment are shown schematically in Fig. 1. The fast neutrons were produced via the  $^7\text{Li}(p,n)^7\text{Be}$  reaction using the Queen's University Van de Graaff accelerator. Each lithium target was produced by evaporating *in vacuo*  $\sim 100$   $\mu\text{g}/\text{cm}^2$  of lithium metal onto a 0.050 cm thick tantalum backing. A  $\sim 20$   $\mu\text{g}/\text{cm}^2$  layer of gold was evaporated over the lithium to protect it from water vapor during the transfer from the evaporator to the beam line. The target was mounted at  $45^\circ$  with respect to the beam, and was water cooled. Protons at energies of 1.93, 2.30, 2.77, 3.22, and 3.68 MeV were used, producing neutrons with maximum energies of 0.14, 0.57, 1.07, 1.53, and 2.00 MeV, respectively. Proton beam currents of  $\sim 15$   $\mu\text{A}$  were used to produce neutron beams between  $2$ – $8 \times 10^7$  neutrons  $\text{s}^{-1}$  at the gas target. At each proton energy, a 48 h run was done with the  $^3\text{He}$

gas in place, followed by a 24 h background run with the gas removed.

Nearly monoenergetic neutrons are produced between proton energies of 1.92 and 2.37 MeV using the  $^7\text{Li}(p,n_0)^7\text{Be}(\text{g.s.})$  reaction. Above 2.37 MeV, a second group of neutrons is produced through the  $^7\text{Li}(p,n_1)^7\text{Be}(0.43 \text{ MeV})$  reaction. However, the intensity of the second group in the forward direction (into the  $^3\text{He}$  gas target) is relatively weak, never exceeding  $\sim 12\%$  of the ground state group over the energy range of the present experiment. Corrections for the effects of this second group were made and are described below.

The total number of neutrons produced during each data run was determined off line from measurements of the  $^7\text{Be}$  activity within each lithium target. The unstable  $^7\text{Be}$  produced in the target decays by electron capture with a half-life of 53.3 d, 10.52% of these decays being to the first excited state of  $^7\text{Li}$  at 478 keV [25]. The activity of 478 keV gamma rays from each target was measured using a HPGe detector. The results of the activity measurements were compared to the expected values calculated from the integrated beam current, the target thickness measured with a quartz crystal monitor during target production ( $\pm 10\%$  uncertainty), and the  $^7\text{Li}(p,n)$  cross sections of Liskien and Paulsen [26] ( $\pm 5\%$  uncertainty). In each case, the measured and calculated results agreed to within the uncertainties.

While removing the lithium target used in the  $E_p = 2.77$  MeV run with the  $^3\text{He}$  gas in place, some water accidentally contacted part of the target outside of the area hit by the proton beam. It is not known how much, if any, of the  $^7\text{Be}$  was washed off; however, the measurements of the activities of lithium flakes from other targets indicate that most of the  $^7\text{Be}$  was implanted in the target backing upon production. Hence, it is not expected that much of the  $^7\text{Be}$  was lost. A conservative estimate of the loss is  $10 \pm 10\%$ , based on the affected area of the target. This estimate was used to correct the deduced number of  $^7\text{Li}(p,n)$  reactions which had occurred in the target, and thus, the number of neutrons that passed through the  $^3\text{He}$  gas (see Table III).

The gas target was a cylindrical  $^3\text{He}$  proportional counter, 5.0 cm in diameter and 25 cm long. The fill gas was a mixture of  $^3\text{He}$  ( $4.54 \times 10^{20}$  atoms/ $\text{cm}^3$ ) and  $\text{CO}_2$  ( $0.15 \times 10^{20}$  molecules/ $\text{cm}^3$ ). The walls of the counter were made from 0.5 mm stainless steel. The  $^3\text{He}$  counter was encased in 1.2 mm of cadmium metal to shield it from thermal neutrons. During the background runs, the cadmium casing was left in place and the  $^3\text{He}$  counter was replaced by an equal mass of steel pipe.

The  $^3\text{He}$  proportional counter was used to measure the effects of the passive shielding on the neutron energy distribution in the gas target. The shielding geometry was changed in an effort to produce measurable differences in the neutron energy spectra. No effects of neutron scattering from the shielding were detected within a statistical uncertainty of 0.5%. Hence, the contribution of these neutrons to the  $^3\text{He}(n,\gamma)$  reaction was assumed to be negligible.

The results of previous studies of the  $^3\text{He}(n,\gamma)$  reaction for neutrons in the energy range 10–120 keV [27]

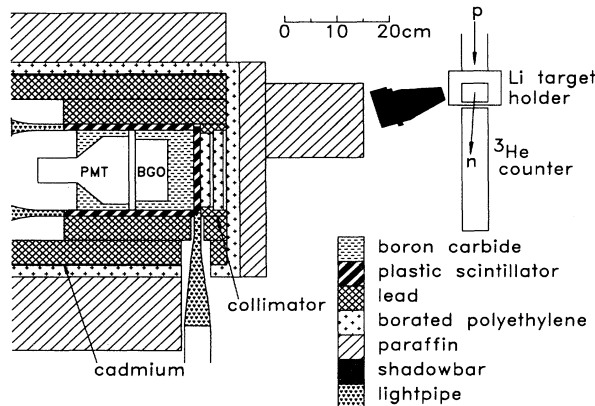


FIG. 1. Schematic top view of the spectrometer and target systems.

and at 9.0 MeV [28] indicate that, for neutrons in the energy range of the present experiment, the reaction goes predominately by  $p$ -wave capture and the gamma rays are emitted over a dipole angular distribution. Thus, to maximize the gamma ray detection efficiency the spectrometer was placed facing the center of the gas target at an angle of  $90^\circ$  with respect to the proton beam direction. The spectrometer consisted of a  $\phi 127 \text{ mm} \times 76 \text{ mm}$  bismuth germanate oxide (BGO) scintillator for detecting the gamma rays, an active shield of plastic scintillator for vetoing cosmic ray muon events, and passive shielding for attenuating neutrons and background capture gamma rays. The BGO crystal was chosen for its high gamma ray detection efficiency, and for its low sensitivity to neutron backgrounds [29,30]. A shadowbar (90% tungsten and 10% nickel by weight) was used to attenuate neutrons and gamma rays from the lithium target emitted in the direction of the spectrometer. A light-emitting diode (LED) light pulser was used to inject a known number of pulses into the BGO crystal/photomultiplier tube interface to determine the deadtime of the system, and to monitor gain changes during the experiment.

### III. DATA ACQUISITION

In the following, the measurements performed with the  ${}^3\text{He}$  target in place and with the target removed are referred to as *gas in* and *gas out* runs, respectively. The shadowbar was removed before and after each run so that the gamma rays produced via the  ${}^7\text{Li}(p,\gamma)$  reaction ( $Q$  value of 17.24 MeV) could be used to calibrate the energy response of the system. Figure 2 shows the energy spectrum at  $E_p=2.30 \text{ MeV}$ , collected with conventional electronics and with the shadowbar removed. The count rate above  $\sim 1 \text{ MeV}$  was typically  $(10\text{--}20) \times 10^3$  counts per second, and was predominately due to the neutron capture background. Each pulse was clipped to  $\sim 350 \text{ ns}$  to reduce pileup.

During data collection, clipped pulses that were not vetoed by the cosmic ray suppression shield were digitized using a Lecroy 9410 digital storage oscilloscope. The dis-

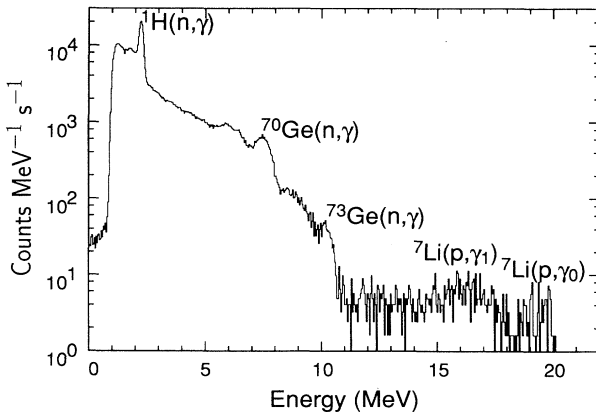


FIG. 2. The  ${}^7\text{Li}(p,\gamma)$  spectrum and background. The discriminator level was set at  $\sim 1 \text{ MeV}$ .

criminator level was set at  $\sim 13 \text{ MeV}$  to reduce the system dead time and the amount of memory required to store the digitized pulses. The stored pulses were later processed off line by computer. In the processing, the charge of each pulse was determined, corrected for gain shifts, and used to construct an energy spectrum. Pile-up events were identified by the shapes of the digitized pulses, and accounted for  $\sim 30\%$  of the total number of counts in the region of interest above 15.4 MeV. These pulses were deconvoluted, and the charges of the separate pulses were determined. Signals produced by the LED light pulser were clearly identifiable, allowing accurate determination of the system dead time. Afterpulses were also easily identified and discarded. A detailed description of the electronics and digital pulse processing can be found in Refs. [23,24].

### IV. CALCULATION OF THE SPECTROMETER RESPONSE FUNCTION

A Monte Carlo simulation of the experiment was developed to determine the response function of the spectrometer for each run. The program simulates the transport of particles in a geometry similar to that of the present experiment. In the calculation, neutrons were tracked through the lithium target holder and  ${}^3\text{He}$  counter, and gamma rays produced via the  ${}^3\text{He}(n,\gamma)$  reaction were tracked out of the  ${}^3\text{He}$  counter and through the materials in the spectrometer around the BGO crystal. Within the BGO crystal itself, the secondary radiation (electrons, positrons, and photons) produced by each gamma ray was also tracked. This was done to reproduce the low-energy tail in the detector response function, as the tail is produced predominately by events in which some of the energy is carried out of the crystal by escaping bremsstrahlung [31]. The latter part of the program was based on the Monte Carlo simulation developed by Varley *et al.* [32] for calculating the response functions of germanium detectors to electrons, positrons, and photons in the energy region of 50 keV to 12 MeV. That program was modified to allow for the tracking of medium-energy particles in BGO. The details of the modifications are given in Ref. [23].

The thicknesses of the gold and lithium layers given in Table I were used to calculate the proton energy loss through each target ( $\leq 20 \text{ keV}$ ). The starting energy and

TABLE I. Neutron production target details, and the maximum energies  $E_0$  and  $E_1$  of the ground state and first excited state neutron groups, respectively. The gold and lithium thicknesses are accurate to  $\sim \pm 10\%$ .

$E_p$ (MeV)	Beam current ( $\mu\text{A}$ )	Gold thickness ( $\mu\text{g}/\text{cm}^2$ )	Li thickness ( $\mu\text{g}/\text{cm}^2$ )	$E_0$ (MeV)	$E_1$ (MeV)
1.93	16	25	140	0.135	
2.30	15.5	42	140	0.571	
2.77	17	25	170	1.068	0.576
3.22	13	34	170	1.530	1.060
3.68	13	25	170	1.999	1.538

direction of each neutron generated via the  ${}^7\text{Li}(p, n)$  reaction was picked from the distributions of Liskien and Paulsen [26]. The neutrons were tracked through the target systems until they escaped or were captured. For capture via the  ${}^3\text{He}(n, \gamma)$  reaction, the cross section at energy  $E_n$  (MeV) was assumed to be  $\sigma_{n, \gamma} = \sigma_0 f_\sigma(E_n)$ , where  $\sigma_0$  is the cross section at the maximum neutron energy  $E_0$  produced in the  ${}^7\text{Li}(p, n_0){}^7\text{Be}(\text{g.s.})$  reaction at each proton energy, and the energy dependence  $f_\sigma(E_n)$  is

$$f_\sigma(E_n) = C\sqrt{E_n}(20.58 + 0.75E_n)^3 e^{-3E_n/4\epsilon}, \quad (1)$$

where  $\epsilon \approx 6$  MeV, and the constant  $C$  is chosen so that  $f_\sigma(E_0) = 1$ . This energy dependence was derived by Flowers and Mandl [33] assuming a direct  $E1$  transition and central nucleon-nucleon forces. Although the theory is crude, the shape of the cross section derived from it over the energy range  $E_n = 0.15$ – $2.0$  MeV agrees well with the preliminary results of a refined resonating group model calculation [34]. Hence, the assumed energy dependence of the cross section is probably accurate enough over the neutron energy spreads of the present measurement [ $\Delta E_n \leq 40$  keV full width at half maximum (FWHM)].

For a  ${}^3\text{He}$  density of  $4.54 \times 10^{20}$  atoms/cm<sup>3</sup> and a  ${}^3\text{He}(n, \gamma)$  cross section of  $100 \mu\text{b}$ , the probability of radiatively capturing the neutron in 25 cm of gas is  $\sim 10^{-6}$ . With the usual analog Monte Carlo techniques, generating gamma rays at such a low rate would result in excessive computational times for calculating response functions with reasonable statistics. Thus, to increase the number of histories in which a  ${}^3\text{He}(n, \gamma)$  reaction occurred during the calculations, a *forced collision* technique [35] was used under a thin target assumption. Neutrons were tracked as if the  ${}^3\text{He}(n, \gamma)$  reaction did not exist; however, each time a neutron passed through the  ${}^3\text{He}$  gas, a gamma ray was produced with a weighting factor that was proportional to the probability of the reaction occurring. The probability was  $(1 - e^{-\Sigma_{n, \gamma}(E_n)\ell}) \simeq \Sigma_{n, \gamma}(E_n)\ell$ , where  $\Sigma_{n, \gamma}(E_n)$  is the macroscopic cross section for the  ${}^3\text{He}(n, \gamma)$  reaction, and  $\ell$  is the neutron path length through the  ${}^3\text{He}$  gas. From Eq. (1),  $\Sigma_{n, \gamma}(E_n) = \Sigma_{n, \gamma}(E_0)f_\sigma(E_n)$ , where  $E_0$  is the maximum neutron energy produced in the  ${}^7\text{Li}(p, n_0)$  reaction. Thus, the probability of a neutron reacting via the  ${}^3\text{He}(n, \gamma)$  reaction was approximated by  $\Sigma_{n, \gamma}(E_n)\ell = f_\sigma(E_n)(\ell/L)[\Sigma_{n, \gamma}(E_0)L]$ , where  $L$  is the maximum pathlength through the  ${}^3\text{He}$  counter. Since  $\Sigma_{n, \gamma}(E_0)$  was unknown during the simulations, and only relative weighting is required for calculating the shape of a spectrum, each gamma ray was weighted by

$$w_\gamma = f_\sigma(E_n)(\ell/L). \quad (2)$$

Because of the small cross section, the position of the radiative capture event was chosen from a uniform distribution along the path length through the  ${}^3\text{He}$ . The emission angle  $\theta$  of the gamma ray relative to the direction of the neutron was chosen from an isotropic distribution in the center-of-mass reference frame so that the effective solid angle of the detector could be simply calculated. A correction to account for the dipole distri-

bution of the gamma rays was applied afterwards. The gamma rays were then tracked through the system until they escaped or were captured.

The simulations were run until there were  $\sim 50 \times 10^3$  events in which  $\geq 0.6$  MeV was deposited in the BGO crystal. The distribution of emission angles of the gamma rays aimed at the BGO crystal that generated counts in the region of interest above 15.4 MeV was calculated in each case. Figure 3 shows the results from the  $E_p = 2.30$  MeV calculation, and is typical of the results from the other calculations. The distributions are slightly skewed to angles below  $90^\circ$  ( $\bar{\theta} \simeq 84.5^\circ$ ) due to the flux of neutrons being greatest in the part of the  ${}^3\text{He}$  counter closest to the neutron production target. Spectra of the total energy deposited in the BGO crystal over each event were also calculated, and were subsequently smeared to match the resolution of the experimental data. Figure 4 shows the smeared spectrum for the  $E_p = 2.30$  MeV calculation, and is typical of the results generated in the other calculations.

The neutron tracking part of the simulations indicates that the fraction of neutrons started in the direction of the  ${}^3\text{He}$  counter that interacted between the neutron production target and the gas target ranged from 52% for the  $E_p = 1.93$  MeV run to 27% for the  $E_p = 3.68$  MeV run. Some of the neutrons that interacted were forward scattered into the  ${}^3\text{He}$  gas, and produced gamma rays through the  ${}^3\text{He}(n, \gamma)$  reaction. The Monte Carlo simulations predict that the fraction of gamma rays produced by scattered neutrons ranged from 26% for the  $E_p = 1.93$  MeV run to 12% for the  $E_p = 3.68$  MeV run.

The gamma ray tracking part of the simulation indicates that about 52% of the gamma rays emitted toward the BGO crystal entered the detector without interacting in the shielding materials. Of these, about 70% deposited at least 15.4 MeV of energy in the crystal to produce counts in the region of interest of the spectrum. Another  $\sim 1\%$  of the gamma rays emitted toward the BGO crystal were scattered in the shielding material before depositing at least 15.4 MeV of energy in the detector. Hence,  $\sim 37\%$  of the gamma rays emitted toward the crystal produced

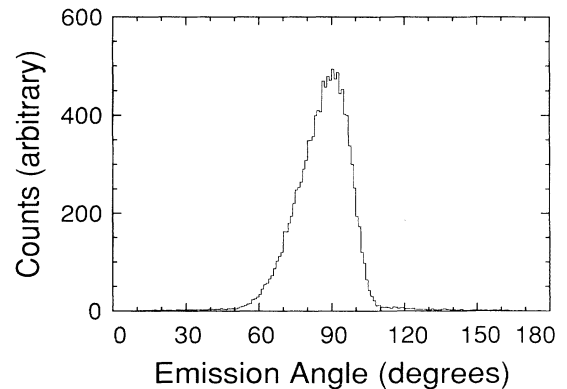


FIG. 3. The calculated distribution of emission angles in the laboratory frame of reference for gamma rays that deposited at least 15.4 MeV in the BGO crystal, from the  $E_p = 2.30$  MeV calculation.

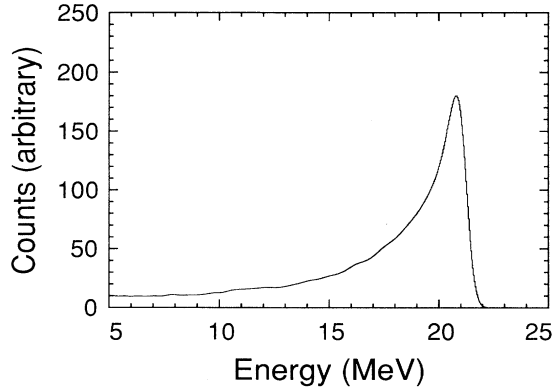


FIG. 4. The Monte Carlo simulated energy spectrum for the  ${}^3\text{He}(n,\gamma)$  reaction at  $E_p=2.30$  MeV, smeared to match the resolution of the experimental data.

counts in the region of interest of the spectrum. Gamma rays that were not emitted toward the BGO crystal but were scattered into the detector accounted for less than 0.34% of the total number of counts in the region of interest. Hence, these gamma rays were ignored in the calculations of the distributions of emission angles of the gamma rays that were detected, and of the effective solid angle of the BGO crystal.

The tracking of photons, electrons, and positrons in the Monte Carlo simulations was tested by comparing the calculated and experimental response functions for gamma rays produced in resonance reactions. The 992 keV resonance of the  ${}^{27}\text{Al}(p,\gamma){}^{28}\text{Si}$  reaction [36] and the 441 keV resonance of the  ${}^7\text{Li}(p,\gamma){}^8\text{Be}$  reaction [25] were used to produce 10.76 and 17.6 MeV gamma rays, respectively. For the  ${}^7\text{Li}(p,\gamma){}^8\text{Be}$  reaction, the recommended value of the cross section at resonance  $\sigma_R$  [25] is based on the work of Fowler and Lauritsen [37], who measured the  $(\gamma_0 + \gamma_1)$  thick target yield  $Y_{\text{max}}(\infty)$  from a lithium target (92.6%  ${}^7\text{Li}$ ) to be  $1.90 \times 10^{-8} \gamma/\text{proton}$  (corrected for the nonresonant background), and the width to be  $\Gamma = 12$  keV (no uncertainties on the results were given). Fowler and Lauritsen used the expression for the cross section at resonance

$$\sigma_R = \frac{2\varepsilon Y_{\text{max}}(\infty)}{\pi\Gamma} \quad (3)$$

with a stopping cross section of  $\varepsilon = 5.95 \times 10^{-15}$  eV cm<sup>2</sup>/ ${}^7\text{Li}$  atom to deduce a value of 6.0 mb for  $\sigma_R$ . However, the presently accepted value for  $\varepsilon$  is  $4.88 \times 10^{-15}$  eV cm<sup>2</sup>/ ${}^7\text{Li}$  atom [38]. Using this value for  $\varepsilon$  and  $\Gamma = 12.2$  keV [25], along with the thick target yield result of Fowler and Lauritsen [37], a value of 4.83 mb is obtained for  $\sigma_R$ . Figures 5 and 6 show that the results of the simulations and experiments are in good agreement for both reactions. The Monte Carlo program developed for the present work was also checked against the EGS4 code [39] for the case of a bare  $\phi 127$  mm  $\times$  76 mm BGO crystal situated 30 cm from a point isotropic source of 10.76 MeV gamma rays. The spectra generated in the calculations agreed to within the statistical uncertainties.

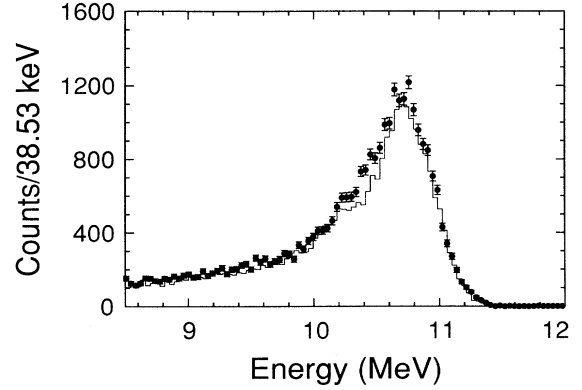


FIG. 5. Measured (points) and calculated (histogram) spectra for 10.76 MeV gamma rays produced via the  ${}^{27}\text{Al}(p,\gamma){}^{28}\text{Si}$  reaction at  $E_p=992$  keV. The calculated spectrum is scaled to the expected number of gamma rays produced in the target, which is known to an accuracy of  $\pm 6\%$ .

From the results of the tests, it appears that the physics embodied in the program for gamma ray tracking simulates the actual interactions with reasonable accuracy. The systematic uncertainty in the results of the simulations for the response function for gamma rays produced in the  ${}^3\text{He}(n,\gamma)$  reaction is estimated to be  $\sim \pm 5.7\%$ , and is mostly due to the uncertainty in the attenuation of the neutron beam through the steel target holder.

## V. DATA ANALYSIS

The raw data after the digital pulse processing are shown in Fig. 7. For comparison, the *gas out* data have been normalized to the same number of neutrons produced during the *gas in* run. The peak produced by the gamma rays of interest from the  ${}^3\text{He}(n,\gamma)$  reaction is located at  $\sim 21$  MeV. Counts appearing well below the

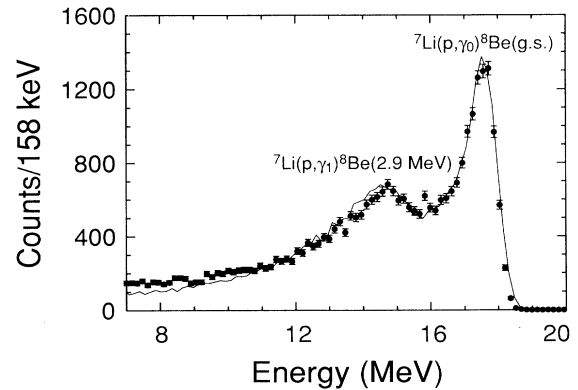


FIG. 6. Measured (points) and calculated (histogram) spectra for  $(\gamma_0 + \gamma_1)$  produced via the  ${}^7\text{Li}(p,\gamma){}^8\text{Be}$  reaction at  $E_p=441$  keV. The calculated spectrum is scaled to the expected number of gamma rays produced in the target, which is known to an accuracy of  $\pm 5.3\%$ .

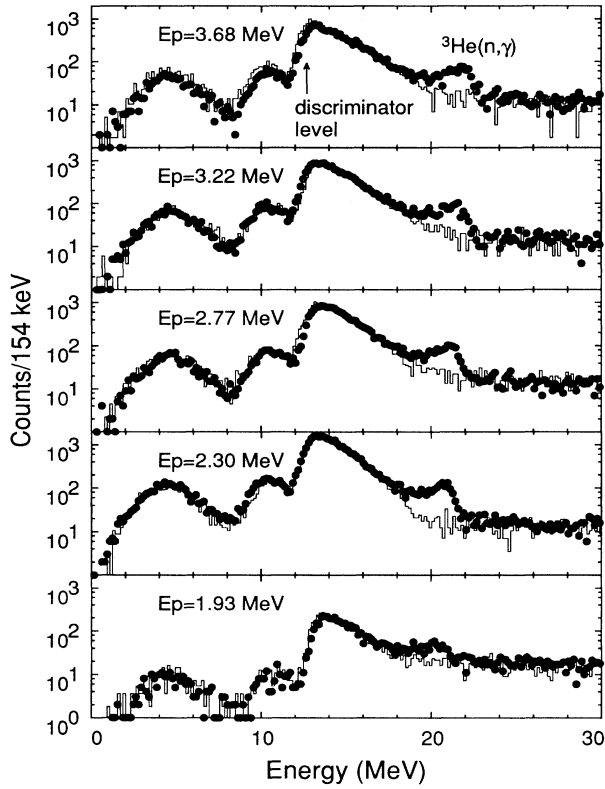


FIG. 7. The raw data from each run. The *gas in* data are shown as points, and the *gas out* data are shown as histograms. The *gas out* data have been renormalized, as explained in the text. The discriminator level was set at  $\sim 13$  MeV, and counts below this energy are due to deconvoluted pileup events.

discriminator level at  $\sim 13$  MeV are due to deconvoluted pileup events.

The analyses of the spectra were confined to a region above 15.4 MeV to avoid effects of the discriminator on the shape of the spectra near the threshold. The raw spectra were corrected for deadtime losses ( $\leq 0.5\%$ ), as determined using the LED light pulser. The cosmic ray component, measured over a period of 119 h with the accelerator off, was subtracted from each spectrum after normalizing to the number of counts in the region above the  ${}^3\text{He}(n, \gamma)$  peak. The remaining background was due predominately to gamma rays from the  ${}^7\text{Li}(p, \gamma)$  reaction that leaked through the shadowbar, and pileup from  $(n, \gamma)$  events in the spectrometer. The line shape of this background for each run was obtained by fitting the cosmic ray subtracted *gas out* spectrum with a Gaussian plus quadratic function. The background spectra and the results of the fits are shown in Fig. 8.

The next step was to subtract the contribution due to the neutrons from the  ${}^7\text{Li}(p, n_1){}^7\text{Be}(0.43 \text{ MeV})$  reaction. This applied to the data at  $E_p = 2.77, 3.22,$  and  $3.68$  MeV. To calculate the contribution in each case, a Monte Carlo simulation was done for the response of the spectrometer to gamma rays produced by the same number of neutrons from the  ${}^7\text{Li}(p, n_1){}^7\text{Be}(0.43 \text{ MeV})$  reaction as was

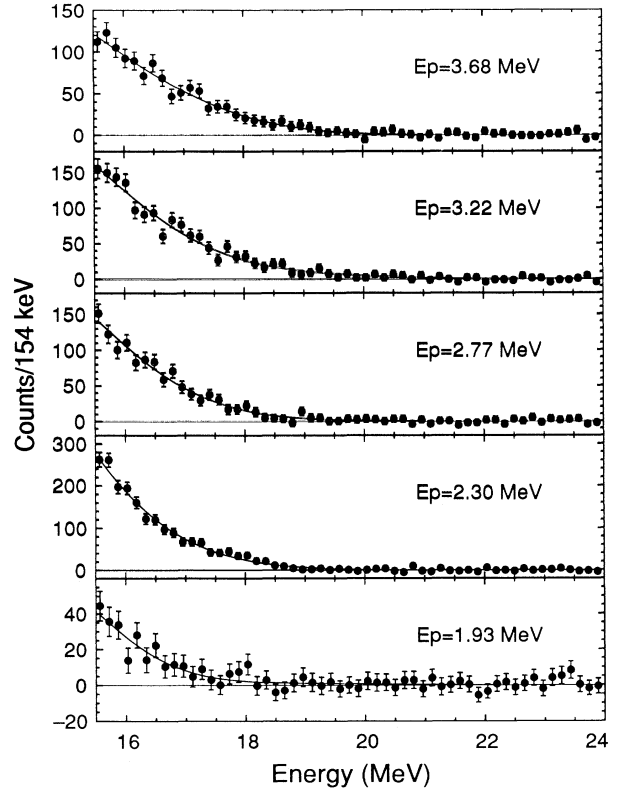


FIG. 8. The dead time corrected and cosmic ray subtracted *gas out* spectra for each run (points), along with the results of fits to a Gaussian plus a quadratic background (lines).

produced in the experiment. The latter quantity was calculated from published cross sections for the  ${}^7\text{Li}(p, n_1)$  and  ${}^7\text{Li}(p, n_0)$  reactions [26], and from the activity of the  ${}^7\text{Be}$  produced in the lithium targets. Except for the kinematics of the production of the neutrons, the simulations were identical to those done for the neutrons from the  ${}^7\text{Li}(p, n_0){}^7\text{Be}(\text{g.s.})$  reaction. The absolute cross section for the  ${}^3\text{He}(n, \gamma)$  reaction used in the calculations was that given by Eq. (1), with  $\sigma_0 = 1 \mu\text{b}$  in each case. Table I shows the calculated maximum energy  $E_1$  of the  $n_1$  group neutrons for each measurement. The proton energies were chosen so that the energy of the  $n_1$  group in any measurement was close to the energy of the  $n_0$  group in the previous measurement. Hence, the contribution subtracted from the measured  ${}^3\text{He}(n, \gamma)$  spectra was that

TABLE II. The number of  ${}^3\text{He}(n, \gamma)$  detected events,  $N$ , and the number of gamma rays,  $N_\gamma$ , emitted in the direction of the BGO crystal for each run.

$E_p$ (MeV)	$N$	$N_\gamma$
1.93	$389 \pm 46(\text{stat})$	$1089 \pm 130(\text{stat}) \pm 15(\text{syst})$
2.30	$1784 \pm 66(\text{stat})$	$4872 \pm 180(\text{stat}) \pm 68(\text{syst})$
2.77	$1417 \pm 61(\text{stat})$	$3813 \pm 160(\text{stat}) \pm 53(\text{syst})$
3.22	$1137 \pm 60(\text{stat})$	$3041 \pm 160(\text{stat}) \pm 43(\text{syst})$
3.68	$928 \pm 54(\text{stat})$	$2461 \pm 140(\text{stat}) \pm 34(\text{syst})$

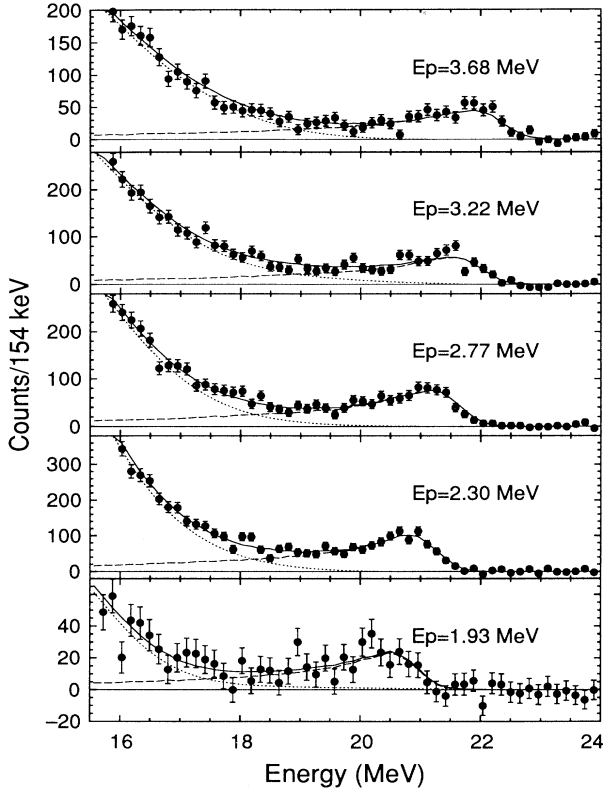


FIG. 9. The dead time corrected and cosmic ray subtracted *gas in* spectra for each run (points). Also shown are the results of the fits to the Monte Carlo simulated  ${}^3\text{He}(n,\gamma)$  line shapes (long dashes) and the background line shapes (short dashes), as well as their sums (solid lines).

calculated with the Monte Carlo simulation, but scaled by the cross section extracted for the  $n_0$  group from the previous measurement. The calculations showed that, at each proton energy, less than 7% of the counts due to gamma rays from the  ${}^3\text{He}(n,\gamma)$  reaction were produced by  $n_1$  group neutrons.

To determine the number of gamma rays from the  ${}^3\text{He}(n,\gamma)$  reaction that were detected during each run,

the corrected *gas in* spectrum was fitted using the background line shape and the Monte Carlo simulated  ${}^3\text{He}(n,\gamma)$  line shape. The results of the fits are shown in Fig. 9, and the number  $N$  of  ${}^3\text{He}(n,\gamma)$  detected events for each run is shown in Table II. The number of gamma rays,  $N_\gamma$ , emitted in the direction of the BGO crystal during each run was then deduced from  $N$  using the detection efficiency calculated in the simulations. As noted previously, the efficiency was  $\sim 37\%$ . The results for  $N_\gamma$  are also shown in Table II.

The differential cross section in the laboratory frame of reference for the  ${}^3\text{He}(n,\gamma)$  reaction averaged over the neutron energies, beam angle spread, and BGO detector solid angle was calculated from  $N_\gamma$  using the expression

$$\langle \sigma(E_n, \theta) \rangle_{E_n, \Delta\Omega} = \frac{N_\gamma}{N_n n_{\text{He}} t \Delta\Omega}, \quad (4)$$

where  $N_n$  is the number of neutrons that passed through the  ${}^3\text{He}$  counter,  $n_{\text{He}}$  is the atomic density of the  ${}^3\text{He}$  gas,  $t$  is the effective target thickness (cm), and  $\Delta\Omega$  is the effective solid angle subtended by the BGO crystal. The Monte Carlo simulation was used to directly calculate both  $\Delta\Omega$  and the probability that each  $n_0$  neutron would pass through the  ${}^3\text{He}$  gas. The product of the latter quantity with the total number of  $n_0$  neutrons produced as deduced from the  ${}^7\text{Be}$  activity measurements gives  $N_n$ . The effective target thickness  $t$  was calculated in the simulations by averaging the path lengths  $\ell$  of the neutrons passing through the  ${}^3\text{He}$  gas.

The averaged differential cross section was expressed as  $\langle \sigma(E_n, \theta) \rangle_{E_n, \Delta\Omega} = C_{E_n} C_{w(\theta)} \sigma(E_0, 90^\circ)$ , where the two constants  $C_{E_n}$  and  $C_{w(\theta)}$  accounted for the effects of the averaging over the neutron energies and photon emission angles, respectively. Using the energy dependence for the cross section derived by Flowers and Mandl [33], the first constant is given by the quantity  $f_\sigma(E_n)$  from Eq. (1) averaged over the neutron energies, that is,

$$C_{E_n} = \langle f_\sigma(E_n) \rangle. \quad (5)$$

The second constant  $C_{w(\theta)}$  corrects for the difference between the angular distribution for the  ${}^3\text{He}(n,\gamma)$  reaction and the isotropic distribution assumed in the Monte

TABLE III. Quantities for computing the differential cross section in the laboratory frame of reference for each run.  $N_n$  is the number of neutrons that passed through the  ${}^3\text{He}$  target,  $\Delta\Omega$  is the effective solid angle of the BGO crystal,  $\langle w_\gamma \rangle$  is the average value of the gamma ray weighting factor, and  $C_{w(\theta)}$  accounts for the averaging of the differential cross section over  $\Delta\Omega$  assuming a dipole angular distribution in the center-of-mass reference frame. The uncertainties on  $\Delta\Omega$ ,  $\langle w_\gamma \rangle$  and  $C_{w(\theta)}$  were insignificant in comparison to the other uncertainties, and were ignored.

$E_p$ (MeV)	$N_n$	$\Delta\Omega$ (sr)	$\langle w_\gamma \rangle$	$C_{w(\theta)}$
1.93	$[7.58 \pm 0.07(\text{stat}) \pm 0.39(\text{syst})] \times 10^{12}$	0.03423	0.16423	0.94972
2.30	$[1.72 \pm 0.02(\text{stat}) \pm 0.09(\text{syst})] \times 10^{13}$	0.03416	0.18557	0.95165
2.77	$[7.84 \pm 0.11(\text{stat}) \pm 0.97(\text{syst})] \times 10^{12}$	0.03432	0.18672	0.95265
3.22	$[5.63 \pm 0.05(\text{stat}) \pm 0.29(\text{syst})] \times 10^{12}$	0.03449	0.18524	0.95455
3.68	$[3.80 \pm 0.04(\text{stat}) \pm 0.20(\text{syst})] \times 10^{12}$	0.03449	0.18578	0.95558

TABLE IV. The differential cross section at  $90^\circ$  in the laboratory frame of reference, and the absolute cross section for the  ${}^3\text{He}(n, \gamma)$  reaction. In both cases, a pure dipole distribution for the gamma rays was assumed.

$E_p$ (MeV)	$E_0$ (MeV)	$\sigma(E_0, 90^\circ)$ ( $\mu\text{b}/\text{sr}$ )	$\sigma_{n,\gamma}(E_0)$ ( $\mu\text{b}$ )
1.93	0.135	$2.29 \pm 0.05(\text{stat}) \pm 0.12(\text{syst})$	$19.2 \pm 2.3(\text{stat}) \pm 1.0(\text{syst})$
2.30	0.571	$4.00 \pm 0.15(\text{stat}) \pm 0.22(\text{syst})$	$33.5 \pm 1.3(\text{stat}) \pm 1.8(\text{syst})$
2.77	1.068	$6.77 \pm 0.30(\text{stat}) \pm 0.84(\text{syst})$	$56.7 \pm 2.6(\text{stat}) \pm 7.1(\text{syst})$
3.22	1.530	$7.54 \pm 0.40(\text{stat}) \pm 0.41(\text{syst})$	$63.1 \pm 3.4(\text{stat}) \pm 3.4(\text{syst})$
3.68	1.999	$8.99 \pm 0.53(\text{stat}) \pm 0.49(\text{syst})$	$75.3 \pm 4.4(\text{stat}) \pm 4.1(\text{syst})$

Carlo simulations, and is given by

$$C_{w(\theta)} = \frac{\int_0^\pi W(\theta)g(\theta)d\theta}{\int_0^\pi g(\theta)d\theta}, \quad (6)$$

where  $W(\theta)$  is the angular distribution for the gamma rays in the laboratory frame of reference, and  $g(\theta)d\theta$  is the distribution of emission angles of the gamma rays that were detected in the BGO crystal as calculated by the Monte Carlo simulation (see, for example, Fig. 3). Using the fact that  $t = \langle \ell \rangle \equiv \langle \ell/L \rangle L$ , where  $L$  is the maximum path length possible (25.9 cm), then

$$t \langle \sigma(E_n, \theta) \rangle_{E_n, \Delta\Omega} = L \langle \ell/L \rangle \langle f_\sigma \rangle C_{w(\theta)} \sigma(E_0, 90^\circ). \quad (7)$$

As described previously, the product of  $f_\sigma$  with  $(\ell/L)$  is the weighting factor  $w_\gamma$  on each gamma ray [see Eq. (2)]. Hence,  $\langle f_\sigma \rangle \langle \ell/L \rangle$  is given approximately by the average value of the weighting factors  $\langle w_\gamma \rangle$  for the gamma rays produced in the calculations. From Eqs. (4) and (7), the differential cross section is then

$$\sigma(E_0, 90^\circ) = \frac{N_\gamma}{N_n n_{\text{He}} L \Delta\Omega C_{w(\theta)} \langle w_\gamma \rangle}. \quad (8)$$

Assuming that the gamma rays are emitted over a dipole distribution, as indicated by previous experiments [27,28], the quantities necessary for computing  $\sigma(E_0, 90^\circ)$  are shown in Tables II and III, and the results for the differential cross section are shown in Table IV. Also, under the same assumption, the total cross section for the  ${}^3\text{He}(n, \gamma)$  reaction  $\sigma_{n,\gamma}(E_0)$  was computed, and is listed in Table IV for each energy.

## VI. DISCUSSION

The results of the present measurement for  $\sigma_{n,\gamma}$  are shown in Fig. 10, along with the  $(n, \gamma)$  results of Ward *et al.* [11], and data deduced from  $(\gamma, n)$  measurements [10,19,40] near the threshold for the reaction. Also shown in the figure is the  $(n, \gamma)$  cross section deduced from the  $(\gamma, n)$  cross section recommended by Calarco *et al.* [9]. Unfortunately, the  $(\gamma, n)$  data and the recommended cross section are not accurate near the threshold for the reaction, i.e., over the energy range of the present experiment. For comparison, it is necessary to extend the present results using a suitable theory to higher energies ( $E_n > 5$  MeV) where the other results are more dependable. Recently, Unkelbach and Hofmann [7] performed a

refined resonating group model (RRGM) calculation of the two-body photodisintegration cross sections on  ${}^4\text{He}$  for  $E_\gamma = 21.4\text{--}50$  MeV. The results are in agreement with the experimental photodisintegration cross sections that yield  $R_\gamma \approx 1.1$  [10,11,20,21], and with electrodisintegration cross sections measured at Mainz [18]. Also, the calculated polarization observables for the  ${}^3\text{H}(\bar{p}, \gamma)$  reaction agree reasonably well with the results of measurements by Wagenaar *et al.* [41]. Hence, it was concluded that a charge symmetry breaking component of the nuclear force is not required to describe most of the recent electro- and photodisintegration results on  ${}^4\text{He}$ . The results of the present experiment agree with the calculated results for  $\sigma_{n,\gamma}$  at low energies if the latter are reduced by  $\sim 5\%$ , as shown in Fig. 10. The calculations were not done for energies below  $E_n = 1.06$  MeV, and so for comparison, the RRGM results were extrapolated to lower energies using the energy dependence given in Eq. (1). The agreement at higher energies between the slightly reduced RRGM results and the data of Berman *et al.* [10] and of Ward *et al.* [11] is also evident in the figure. Thus, with the exception of the diffusion chamber results by Nagornyi *et al.* [19], the results of the RRGM calculations and of the measurements of the  $(n, \gamma)$  or  $(\gamma, n)$  cross sections performed since 1980 are in good agreement. The discrepant result is not unexpected since, as

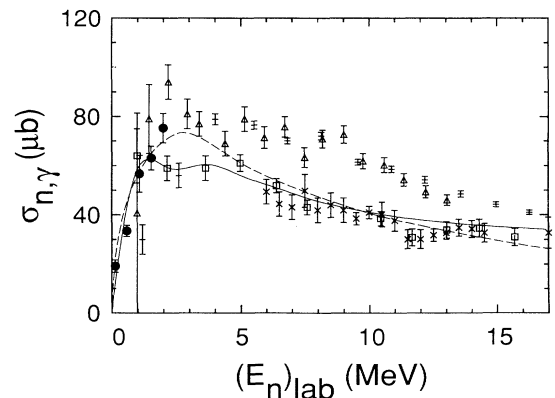


FIG. 10. Measured and calculated values of the cross section for the  ${}^3\text{He}(n, \gamma)$  reaction. The symbols are defined as follows:  $(n, \gamma)$ : (●) the present work; (×) Ward *et al.* [11];  $(\gamma, n)$ : (□) Berman *et al.* [10]; (△) Irish *et al.* [40]; (+) Nagornyi *et al.* [19]; (solid line) Calarco *et al.* [9]; (dashed line) Unkelbach and Hofmann [7] ( $\times 0.95$ ).

pointed out previously [9,10], the published results from experiments [16,42,43] similar to that using the diffusion chamber [19] vary widely for energies below  $E_\gamma=33$  MeV, due probably to the difficulty in measuring the recoiling  ${}^3\text{He}$  atoms at low energies.

## VII. CONCLUSION

In summary, the absolute cross section of the  ${}^3\text{He}(n,\gamma)$  reaction was measured at  $E_n=0.14\text{--}2.0$  MeV to an accuracy of  $\sim\pm 10\%$ . The present results, along with those measured by Berman *et al.* [10] and by Ward *et al.* [11] at higher energies, are described reasonably well by the results of a recent RRGm calculation [7] (reduced by  $\sim 5\%$ ). This confirms the  $(\gamma, n)$  cross section recommended by

Calarco *et al.* [9] over the peak region of the giant dipole resonance. If taken with the recent results for  $\sigma_{\gamma,p}$  measured by Bernabei *et al.* [20] and by Feldman *et al.* [21], the ratio  $R_\gamma = \sigma_{\gamma,p}/\sigma_{\gamma,n}$  is  $\sim 1.1$  over the resonance region, in agreement with the conventional theories [3–7] that include no charge symmetry breaking components in the nuclear force. The sum of the two photodisintegration peak cross sections given above, however, disagrees with the recent result of the elastic photon scattering measurement by Wells *et al.* [22], indicating that there could be some problems with the latter.

We would like to acknowledge the assistance of Dr. H. M. Hofmann and Dr. Jens Miltner who made available the preliminary results of their RRGm calculations using the Bonn potential.

- 
- [1] G.A. Miller, B.M.K. Nefkens, and I. Šlaus, *Phys. Rep.* **194**, 1 (1990).
- [2] F.C. Barker and A.K. Mann, *Philos. Mag.* **2**, 5 (1957).
- [3] J.T. Londergan and C.M. Shakin, *Phys. Rev. Lett.* **28**, 1729 (1972).
- [4] A.H. Chung, R.G. Johnson, and T.W. Donnelly, *Nucl. Phys.* **A235**, 1 (1974).
- [5] D. Halderson and R.J. Philpott, *Phys. Rev. C* **28**, 1000 (1983).
- [6] F.C. Barker, *Aust. J. Phys.* **37**, 583 (1984).
- [7] M. Unkelbach and H.M. Hofmann, *Nucl. Phys.* **A549**, 550 (1992).
- [8] D.R. Tilley, H.R. Weller, and G.M. Hale, *Nucl. Phys.* **A541**, 1 (1992).
- [9] J.R. Calarco, B.L. Berman, and T.W. Donnelly, *Phys. Rev. C* **27**, 1866 (1983).
- [10] B.L. Berman, D.D. Faul, P. Meyer, and D.L. Olsen, *Phys. Rev. C* **22**, 2273 (1980).
- [11] L. Ward, D.R. Tilley, D.M. Skopik, N.R. Roberson, and H.R. Weller, *Phys. Rev. C* **24**, 317 (1981).
- [12] J.E. Perry, Jr. and S.J. Bame, Jr., *Phys. Rev.* **99**, 1368 (1955).
- [13] R.C. McBroom, H.R. Weller, S. Manglos, N.R. Roberson, S.A. Wender, D.R. Tilley, D.M. Skopik, L.G. Arnold, and R.G. Seyler, *Phys. Rev. Lett.* **45**, 243 (1980).
- [14] J.R. Calarco, S.S. Hanna, C.C. Chang, E.M. Diener, E. Kuhlmann, and G.A. Fisher, *Phys. Rev. C* **28**, 483 (1983).
- [15] W.R. Dodge and J.J. Murphy, *Phys. Rev. Lett.* **28**, 839 (1972).
- [16] F. Balestra, E. Bollini, L. Busso, R. Garfagnini, C. Guaraldo, G. Piragino, R. Scrimaglio, and A. Zanini, *Nuovo Cimento A* **38**, 145 (1977).
- [17] T.W. Phillips, B.L. Berman, D.D. Faul, J.R. Calarco, and J.R. Hall, *Phys. Rev. C* **19**, 2091 (1979).
- [18] M. Spahn, Th. Kihm, K.T. Knöpffe, J. Friedrich, N. Voegler, Ch. Schmitt, V.H. Walther, M. Unkelbach, and H.M. Hofmann, *Phys. Rev. Lett.* **63**, 1574 (1989).
- [19] S.I. Nagornyy, Yu.A. Kasatkin, V.A. Zolenko, I.K. Kirichenko, and A.A. Zayats, *Yad. Fiz.* **53**, 365 (1991) [*Sov. J. Nucl. Phys.* **53**, 228 (1991)].
- [20] R. Bernabei, A. Chisholm, S. d'Angelo, M.P. De Pascale, P. Picozza, C. Schaerf, P. Belli, L. Casano, A. Incicchitti, D. Prospero, and B. Girolami, *Phys. Rev. C* **38**, 1990 (1988).
- [21] G. Feldman, M.J. Balbes, L.H. Kramer, J.Z. Williams, H.R. Weller, and D.R. Tilley, *Phys. Rev. C* **42**, R1167 (1990).
- [22] D.P. Wells, D.S. Dale, R.A. Eisenstein, F.J. Federspiel, M.A. Lucas, K.E. Mellendorf, A.M. Nathan, and A.E. O'Neill, *Phys. Rev. C* **46**, 449 (1992).
- [23] R.J. Komar, Ph.D. dissertation, Queen's University at Kingston, 1992.
- [24] R.J. Komar and H.-B. Mak, *Nucl. Instrum. Methods A* (to be published).
- [25] F. Ajzenberg-Selove, *Nucl. Phys.* **A490**, 1 (1988).
- [26] H. Liskien and A. Paulsen, *At. Data Nucl. Data Tables* **15**, 57 (1975).
- [27] V.P. Alfimkov, S.B. Borzakov, G.G. Bunatyan, J. Wierzbicki, L.B. Pikel'ner, and E.I. Sharapov, *Yad. Fiz.* **31**, 21 (1980) [*Sov. J. Nucl. Phys.* **31**, 10 (1980)].
- [28] H.R. Weller, N.R. Roberson, G. Mitev, L. Ward, and D.R. Tilley, *Phys. Rev. C* **25**, 2111 (1982).
- [29] D.M. Drake, L.R. Nilsson, and J. Faucett, *Nucl. Instrum. Methods* **188**, 313 (1981).
- [30] O. Häusser, M.A. Lone, T.K. Alexander, S.A. Kushneriuk, and J. Gascon, *Nucl. Instrum. Methods* **213**, 301 (1983).
- [31] P. Paul, in *Nuclear Spectroscopy and Reactions*, edited by J. Cerny (Academic Press, New York, 1974), Pt. A, p. 345.
- [32] B.J. Varley, J.E. Kitching, W. Leo, J. Miskin, R.B. Moore, K.D. Wunsch, R. Decker, H. Wollnik, and G. Siegert, *Nucl. Instrum. Methods* **190**, 543 (1981).
- [33] B.H. Flowers and F. Mandl, *Proc. R. Soc. London* **A206**, 131 (1951).
- [34] H.M. Hofmann (private communication).
- [35] E.E. Lewis and W.F. Miller, *Computational Methods of Neutron Transport* (Wiley-Interscience, New York, 1984), Chap. 7.
- [36] A. Anttila, J. Keinonen, M. Hautala, and I. Forsblum, *Nucl. Instrum. Methods* **147**, 501 (1977).
- [37] W.A. Fowler and C.C. Lauritsen, *Phys. Rev.* **76**, 314 (1949).
- [38] J.F. Janni, *At. Data Nucl. Data Tables* **27**, 147 (1982).
- [39] W.R. Nelson, H. Hirayama, and D.W.O. Rogers, Stanford Linear Accelerator Center Report No. SLAC-Report-265, 1985.

- [40] J.D. Irish, R.G. Johnson, B.L. Berman, B.J. Thomas, K.G. McNeill, and J.W. Jury, *Can. J. Phys.* **53**, 802 (1975).
- [41] D.J. Wagenaar, N.R. Roberson, H.R. Weller, and D.R. Tilley, *Phys. Rev. C* **39**, 352 (1989).
- [42] A.N. Gorbunov, *Phys. Lett.* **27B**, 436 (1968).
- [43] Yu. M. Arkatov, P.I. Vatsset, V.I. Voloschuk, V.N. Gur'ev, and A.F. Khodyachikh, *Ukr. Fiz. Zh. (Russ. Ed.)* **23**, 1818 (1978).